Application of a Population Balance Approach for Polydispersed Bubbly Flows

Eckhard Krepper[1], Matthias Beyer[1], Thomas Frank[2], Dirk Lucas[1], Horst-Michael Prasser[3]

[1]Forschungszentrum Dresden-Rossendorf (FZD), Institute of Safety Research,
PO Box 510119, D-01314 Dresden, Germany, E.Krepper@fzd.de; M.Beyer@fzd.de; D.Lucas@fzd.de

[2]ANSYS Germany, CFX Development
Staudenfeldweg 12, D-83624 Otterfing Germany, Thomas.Frank@ansys.com;

[3]ETH-Zürich, Department of Mechanical and Process Engineering
ETH-Zentrum, 8092 Zürich, hprasser@ethz.ch

Keywords: Bubbly flow, CFD, Non drag forces, bubble break up, bubble coalescence, population balance, validation

Abstract

A population balance model was developed in close cooperation of ANSYS-CFX and Forschungszentrum Dresden-Rossendorf and implemented into CFX-10 (Frank et al. 2005, Krepper et al. 2007). The current paper presents the application of the model to upward flow in vertical pipes for air/water and for steam/water bubbly flow. Finally the application to a bubbly flow around a half moon shaped obstacle arranged in a 200 mm pipe is shown (see Frank et al. 2007).
Applying the inhomogeneous MUSIG approach a more deep understanding of the flow structure is possible. For upward two phase flow in vertical pipes the core peak in the cross sectional gas fraction distribution could be reproduced very well. For complex flows the general structure of the flow could be well reproduced in the simulations. This test case of the obstacle demonstrates the complicated interplay between size dependent bubble migration and bubble coalescence and break-up effects for real flows. While the closure models on bubble forces, which are responsible for the simulation of bubble migration are in agreement with the experimental observations, clear deviations occur for bubble coalescence and fragmentation. The presently applied models describing bubble fragmentation and coalescence could be proved as weak points in numerous CFD analyses of vertical upward two phase pipe flow. Further work on this topic is under way.

1. Introduction

The multiphase flow regimes found in vertical pipes are dependent on the void fraction of the gaseous phase, which vary from bubbly flows at low fractions to higher void fraction regimes of slug flow, churn turbulent flow, annular flow and finally to droplet flow. In the regime of bubbly and slug flow the multiphase flow shows a spectrum of different bubble sizes. While disperse bubbly flows with low gas volume fraction are mostly mono-disperse, an increase of the gas volume fraction leads to a broader bubble size distribution due to break-up and coalescence of bubbles. Bubbles of different sizes are subject to lateral migration due to forces acting in lateral direction, which is different from the main drag force direction. The bubble lift force was found to change the sign as the bubble size varies. Consequently this lateral migration leads to a radial de-mixing of small and large bubbles and to further coalescence of large bubbles migrating towards the pipe center into even larger Taylor bubbles or slugs.
An adequate modeling approach must to consider all these phenomena. The paper presents a generalized inhomogeneous Multiple Size Group (MUSIG) Model based on the Eulerian modeling framework. Within this model the dispersed gaseous phase is divided into N inhomogeneous velocity groups (phases) and each of these groups is subdivided into M_j bubble size classes. Bubble break-up and coalescence processes between all bubble size classes M_j are taken into account by appropriate models. The model concept is described in detail by Krepper et al. 2007. The current paper shows the capability of the concept by application to different test cases.

2. Nomenclature

C_D	drag coefficient
C_L	lift coefficient
F_B	break-up coefficient
F_C	coalescence coefficient
g	acceleration due to gravity (m s^{-2})
J	superficial velocity (m s^{-1})
M_i	number of subsize fractions in the velocity group i (i = 1..N)
N	number of dispersed velocity groups
P	pressure (Pa)
z	axial position (m)

Greek letters

α	gas volume fraction
ρ	density (kg m^{-3})
σ	surface tension (N m^{-1})

Subscripts

g	gas
l	liquid

3. Upward two phase flow in vertical pipes

Gas-liquid flow in vertical pipes is a very good object for studying the phenomena of two-phase flows. In case of bubbly flows the bubbles move under clear boundary conditions, resulting in a shear field of constant and well-known structure where the bubbles rise for a comparatively long time. This allows studying the lateral motion of the bubbles in a shear flow by comparing gas distributions measured at different heights.

3.1. Air/water flow

In the TOPFLOW test, bubbles were injected from the side walls through 4 mm nozzles into a tube of diameter 195.3 mm. The bubble size distribution near the inlet shows large fractions of large bubbles (Fig. 1, blue size distribution left side). During the upward flow through the tube the size distribution is shifted towards lower values. Thus the development of the bubble size distribution is mainly determined by fragmentation processes. Bubble coalescence plays only a minor role at the flow conditions of the experimental test. Fig. 1 shows the bubble size distribution and radial gas profiles for the test case TOPFLOW 118 for a quite low distance from the gas injection of 0.335 m and at a distance of 7.802 m. Note that only two dispersed phases were defined for the numerical model. 20 sub-size groups were then specified, the first 2 sub-size groups assigned to the first dispersed phase and the other 18 to the second dispersed phase. The bubble size diameter was defined up to 60 mm, the size step between the sub-size groups amounts to 3 mm. Test calculations have shown setting the break-up coefficient to F_B = 0.25 and the coalescence coefficient to F_C = 0.05 yields the best agreement for this flow situation of air/water flow in vertical pipes. Both the shift of the bubble size distribution (Fig. 1 left side) and the core peak gas volume fraction profile are well reproduced by the calculations.

3.2. Steam/water flow at saturation conditions

Besides the air/water tests at the TOPFLOW facility also steam/water tests at pressures up to 6.5 MPa were performed. As a first step the influence of mass transfer by condensation was limited by keeping saturation conditions. Tomiyama (1998) has shown the lift coefficient C_L changing its sign with higher bubble size. For air/water flow at ambient conditions the critical bubble size, for which C_L=0 amounts to be 5.8 mm. The analysis of the correlation for the lift coefficient given by Tomiyama (1998) shows, that with higher pressure the critical bubble size is shifted towards lower values (see Krepper et al. 2007). For steam/water at 6.5 MPa a value of about 3.5 mm and at 15 MPa of about 2 mm was found. These tendencies were confirmed by the TOPFLOW experiments (see Fig. 3, Prasser et al. 2007).

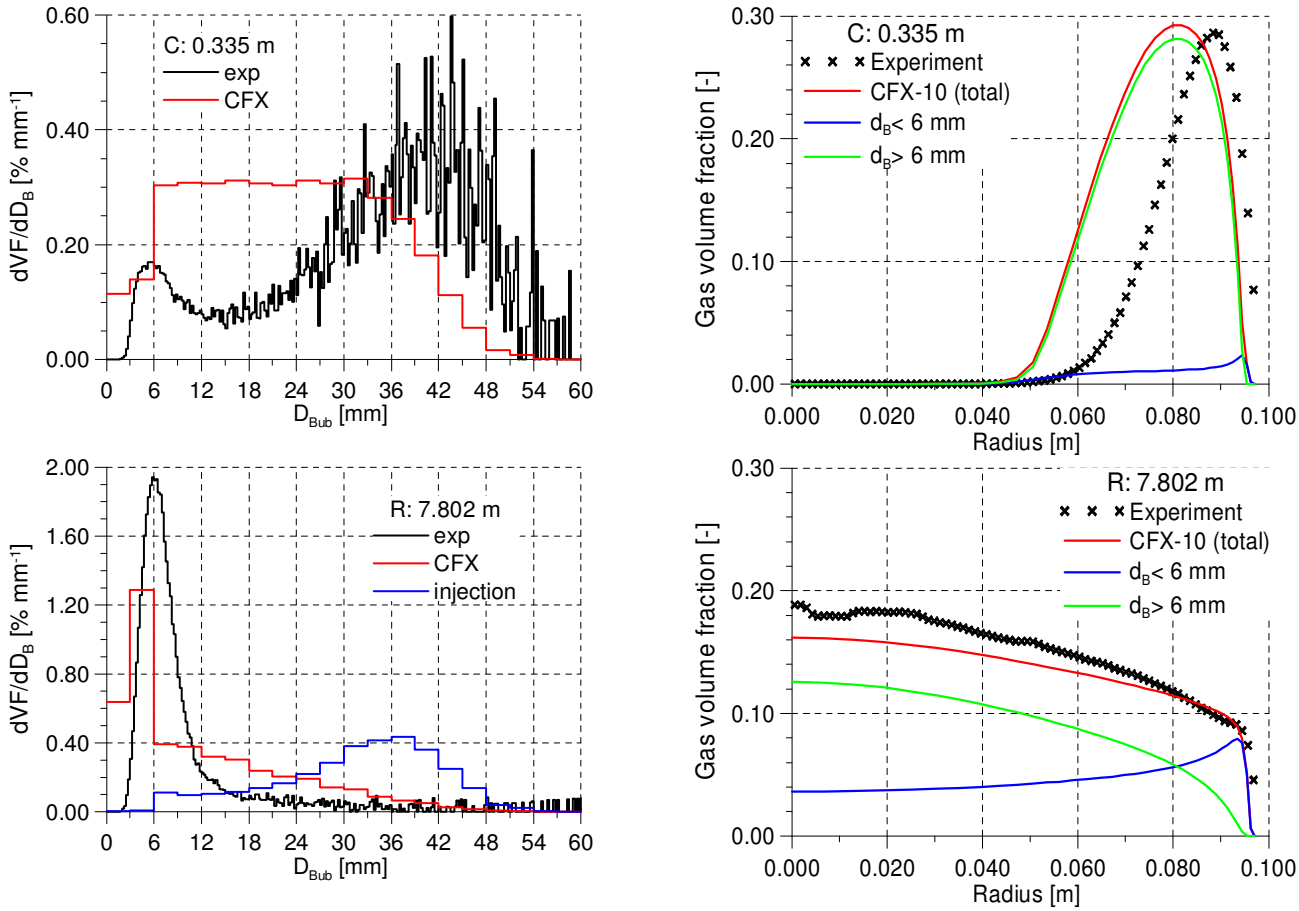

Figure 1: Air/water flow: Bubble size distribution (left) and the radial gas fraction profiles (right) of the simulation of the test case TOPFLOW 118 at the distance levels from the gas injection C and R (J_L = 1.017 m/s; J_G = 0.2194 m/s) (Break-up coefficient F_B = 0.25, Coalescence coefficient F_C = 0.05)

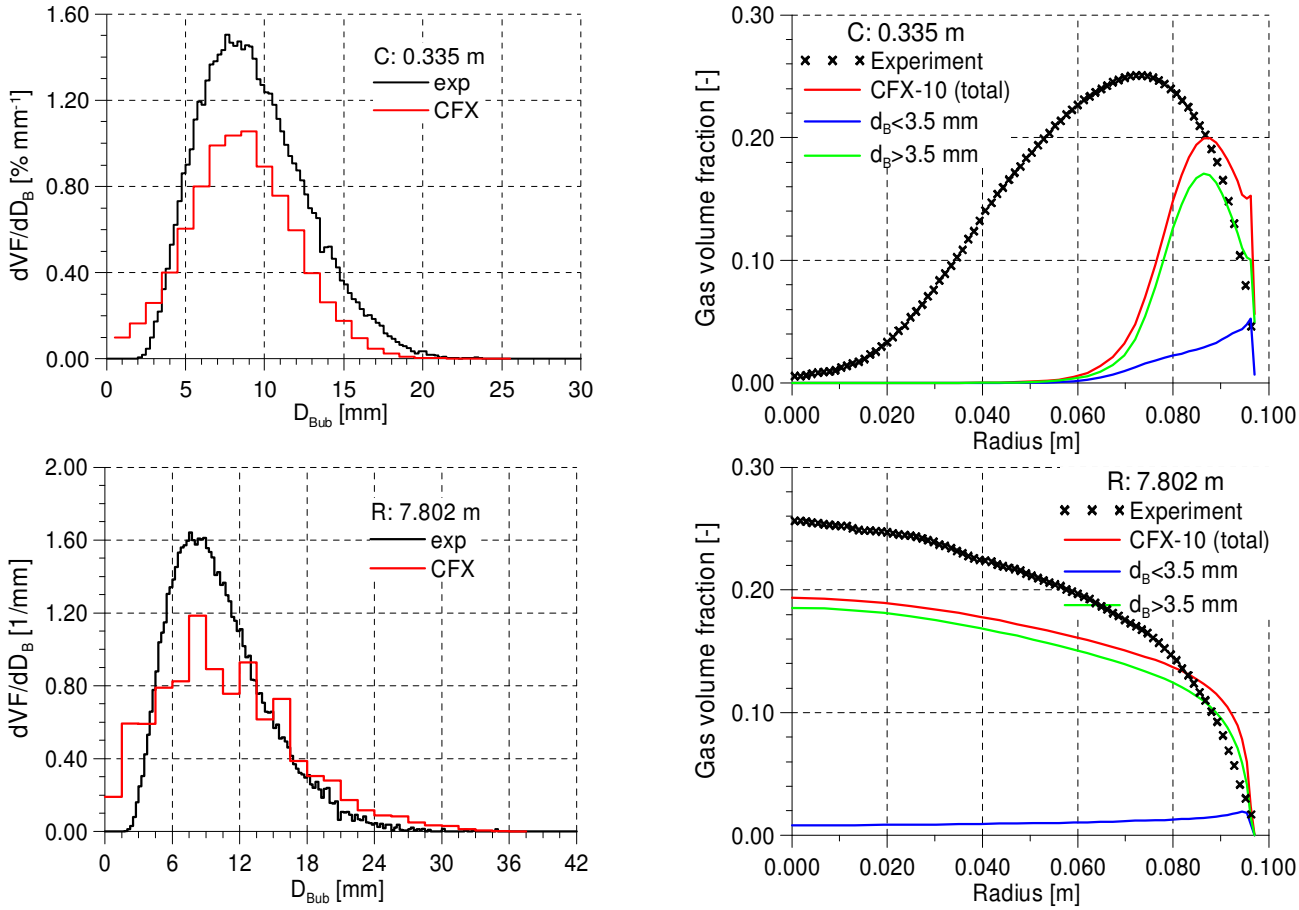

Figure 2: Saturated steam/water flow at 6.5 MPa: Bubble size distribution (left) and the radial gas fraction profiles (right) of the simulation of the test case TOPFLOW 118 at the distance levels from the gas injection C and R (J_L = 1.017 m/s; J_G = 0.2194 m/s) (Breakup coefficient F_B = 0.025, Coalescence coefficient F_C = 0.05)

The changed fluid properties have influence on the calculated turbulence parameters of the liquid. For steam/water at 6.5 MPa the turbulence kinetic energy and the turbulence dissipation are almost doubled compared to air/water flow. Bubble fragmentation and bubble coalescence are strongly influenced by the turbulence dissipation of the liquid phase.

Fig. 2 presents the development of the bubble size distribution and of the radial volume fraction profiles for the steam/water test TOPFLOW-118. At 6.5 MPa steam/water flow with superficial velocities J_L = 1.017 m/s and J_G = 0.12194 m/s was analyzed. 25 sub-size gas fractions assigned to two dispersed phases were simulated. The maximum considered bubble size was 37.5 mm. With equidistant bubble size distribution only the lowest two sub-size gas fractions were assigned to the first dispersed phase. For these flow conditions the critical bubble size for C_L = 0 was 3.5 mm.

Whereas the factor for bubble coalescence was set like in the air/water simulations F_C = 0.05 the fragmentation coefficient lead to a strong overestimation of bubble fragmentation. Consequently this coefficient in the further simulations was remarkably reduced to F_B = 0.025. Fig. 2 shows that applying the models with these tuned coalescence and fragmentation coefficients a reasonable simulation of the development of bubble size distribution and radial gas volume fraction profile is possible.

Compared to the air/water simulations (see Fig. 1) the migration of the bubbles from the injection at the wall to the centre of the tube is simulated slower in the steam/water case. Whereas in the air/water simulations the air moves too fast from the side wall injection into the tube centre, in the steam/water tests the gas migration to the tube centre is underestimated. The reason could be the overestimated turbulent dispersion bubble force in the air/water cases. Caused by the other fluid properties the turbulent bubble dispersion force seems to be underestimated in the steam/water flow tests. Further investigations are necessary.

4. Application of the model for the flow around an obstacle

In the TOPFLOW facility at FZD an experiment was performed, to study the flow field around an asymmetric obstacle. The obstacle had the form of a half moon shaped diaphragm and was arranged in a vertical tube having a diameter of DN200 (see Fig. 3). The experiment is detailed described by Frank et al. 2007. The test is an ideal case for CFD code validation, since the obstacle creates a pronounced three-dimensional two-phase flow field. Curved stream lines, which form significant angles with the gravity vector, a recirculation zone in the wake and a flow separation at the edge of the obstacle are common in industrial components and installations.

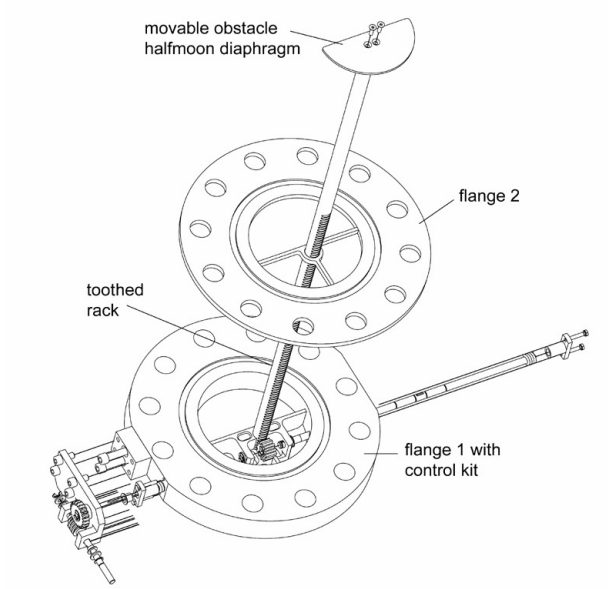

Figure 3: Sketch of the movable obstacle with driving mechanism - a half-moon shaped horizontal plate mounted on top of a toothed rod

The wire-mesh technology was applied to measure the gas volume fraction and the gas velocity in different distances up- and downstream the obstacle. The sensors supplies detailed data on the instantaneous flow structure with a high resolution in space and time. In particular, they allow visualizing the structure of the gas liquid interface.
Pretest calculations using CFX-10 applying a monodispersed bubble size approach were performed for the conditions of test run 074 (J_L = 1.017 m/s, J_G = 0.0368 m/s) (see Prasser et al. 2005, Frank et al. 2007). In the calculation, a fluid domain was modeled 1.5 m upstream and downstream the obstacle. Half of the tube including a symmetry xz-plane was simulated. In the present paper the inhomogeneous model approach was applied to air/water obstacle experiments run 096 (J_L = 1.017 m/s, J_G = 0.0898 m/s) and run 097 (J_L = 1.611 m/s, J_G = 0.0898 m/s). In the presented calculations for run 096 respective run 097 25 respective 20 sub-size gas fractions representing equidistant bubble sizes up to 25 mm respective 20 mm were simulated assigned to 2 dispersed gaseous phases. The first 6 fractions were assigned to the first and the remaining fractions to the second gaseous phase. The bubble size distribution measured at the largest upstream position was set as a boundary condition for the calculation.

4.1. The main observed phenomena

Like in the pretest calculations also the steady-state ANSYS CFX calculations applying the inhomogeneous MUSIG model could reproduce all qualitative details of the flow structure of the two-phase flow field around the diaphragm for the low gas fraction of run 074.
The ANSYS CFX simulation results have been compared to three-dimensional wire-mesh sensor data. The water velocity (Fig. 4) and the total gaseous void fraction are presented (Fig. 5). Like for the pretest calculations also here for the test with higher gas fractions all qualitative details of the structure of the two-phase flow field around the obstacle could be reproduced.

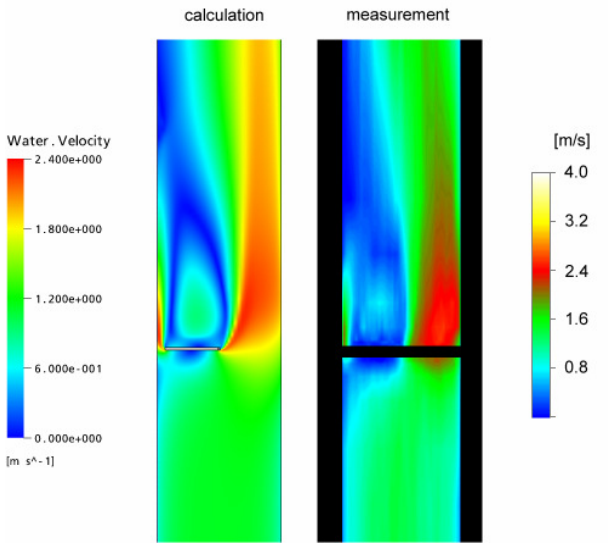

Figure 4: Comparison of time averaged calculated(left) and measured(right) velocities up- and downstream of the obstacle in the air/water test run 096, J_L = 1.017 m/s, J_G = 0.0898 m/s

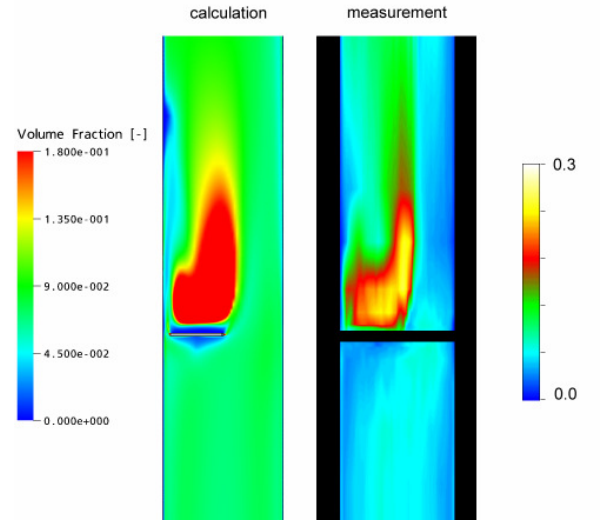

Figure 5: Comparison of time averaged calculated(left) and measured(right) volume fractions up- and downstream of the obstacle in the air/water test run 096

Shortly behind the obstacle a strong vortex of the liquid combined with the accumulation of gas is found. The measured and calculated shape and extension of the recirculation area agree very well. Upstream the obstacle a stagnation point with lower gas content is seen in experiment and calculation. Details, like the velocity

maximum above the gap between the circular edge of the obstacle and the inner wall of the pipe are also found in a good agreement between experiment and calculation. In the undisturbed cross sectional part of the tube a strong jet is established.

4.2. Phenomena in the wake of the obstacle

More detailed understanding of the flow situation can be gained, comparing the results of the inhomogeneous MUSIG model. According to the applied bubble fragmentation model of Luo and Svendsen (1996), bubble fragmentation can be expected in regions showing high turbulence eddy dissipation. Fig. 6 presents maximum values of the turbulence eddy dissipation at the edges of the obstacle. At the same time the applied bubble coalescence model of Prince and Blanch (1990) indicates strong importance of coalescence in regions of bubble accumulation i.e. in the wake behind the obstacle. Both bubble coalescence (see gas accumulation shown in Fig. 5) and bubble breakup (see distribution of turbulence dissipation Fig. 6) partially compensating each other are expected shortly behind the obstacle.

Fig. 7 shows measured cross sectional averaged bubble size distributions upstream (z = -0.52 m), shortly behind (z = 0.08 m) and downstream the obstacle (z = 0.52 m). In the bubble accumulation zone at z = 0.08 m the cross sectional average shows a shift towards larger bubbles. The calculated bubble size distributions (see Fig. 8 for the run 096 and Fig. 9 for run 097) however show a shift of the mean bubble diameter towards smaller bubbles shortly behind the obstacle. In the calculations the bubble breakup is overestimated. This disagreement was found not solvable by simply changing of breakup or coalescence coefficients, which were set here $F_B = F_C = 0.05$. Similar deviations would arise at other locations of the flow domain.

On the one hand the liquid velocity flow field generates a lift force field which transports the small bubbles into the region behind the obstacle (see Fig. 10 for the bubble streamlines and Fig. 11 for the lift force arrows). On the other hand, the air accumulation in this region leads to bubble coalescence and the generation of large bubbles. This phenomenon is underestimated in the calculations. Figs. 10 and 12 show very well small bubbles being transported behind the obstacle. In the experiments larger bubbles are created by coalescence in this region. In the calculations however, bubble coalescence is exceeded in this region by bubble fragmentation. Caused by the lift force large bubbles are redirected into the downstream jet (see Fig. 11). The streamline representation (see Fig. 10) clearly shows this phenomenon for large bubbles already present in the upstream flow.

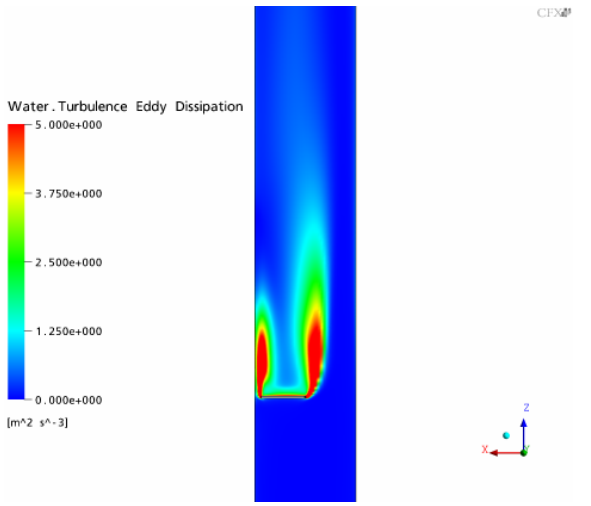

Figure 6: Calculated turbulence eddy dissipation (run 096)

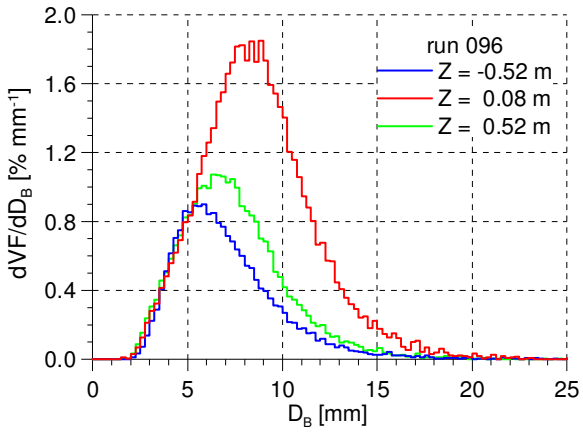

Figure 7: Measured bubble size distribution for run 096

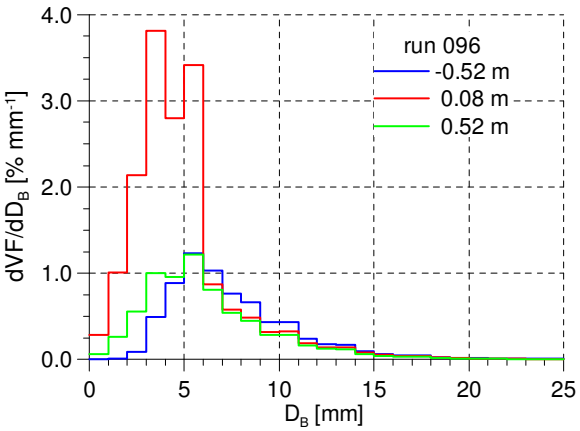

Figure 8: Calculated bubble size distributions for run 096 (J_L = 1.017 m/s, J_G = 0.0898 m/s)

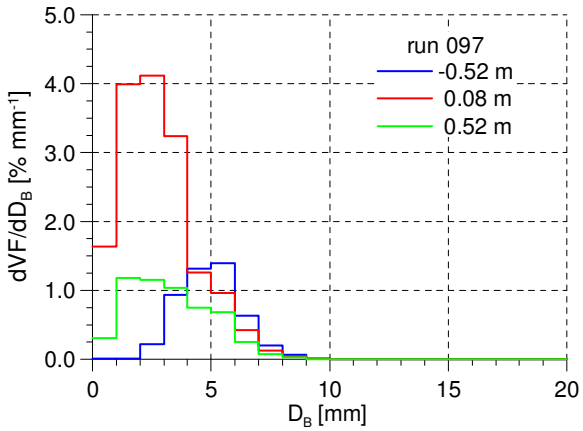

Figure 9: Calculated bubble size distributions for run 097 (J_L = 1.611 m/s, J_G = 0.0898 m/s)

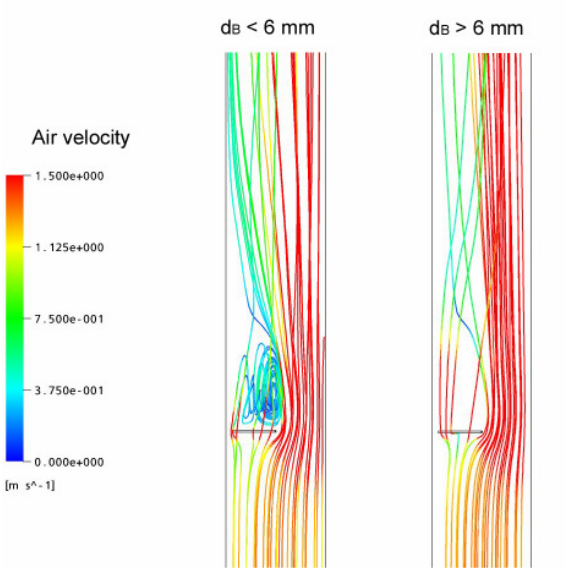

Figure 10: Streamlines for small (left) and large (right) bubbles (run 096)

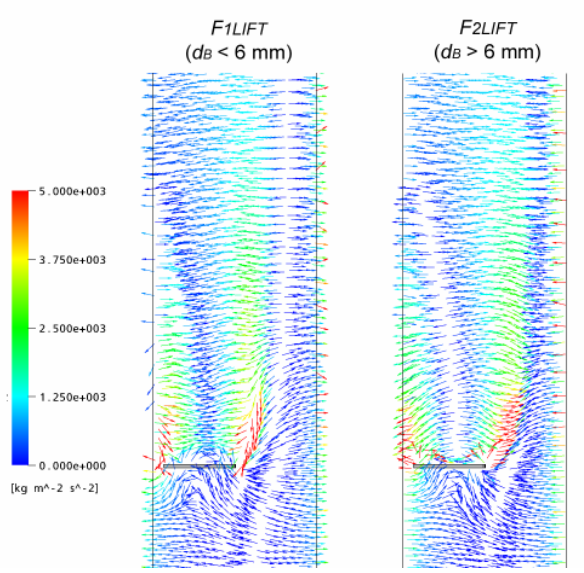

Figure 11: Bubble lift force vectors for the different gas velocity groups (run 096)

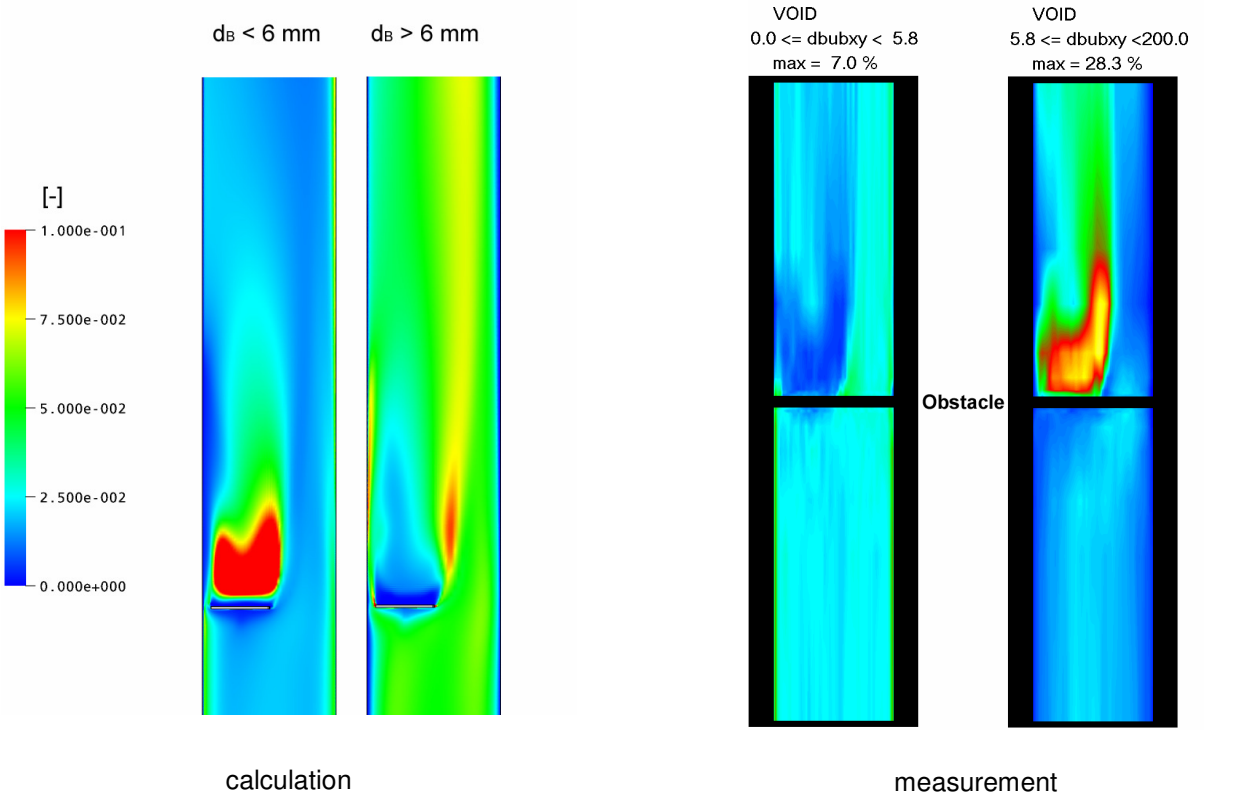

Figure 12: Calculated (left) and measured (right) gas distributions up- and downstream of the obstacle resolved to bubble size classes (run 096: J_L = 1.017 m/s, J_G = 0.0898 m/s)

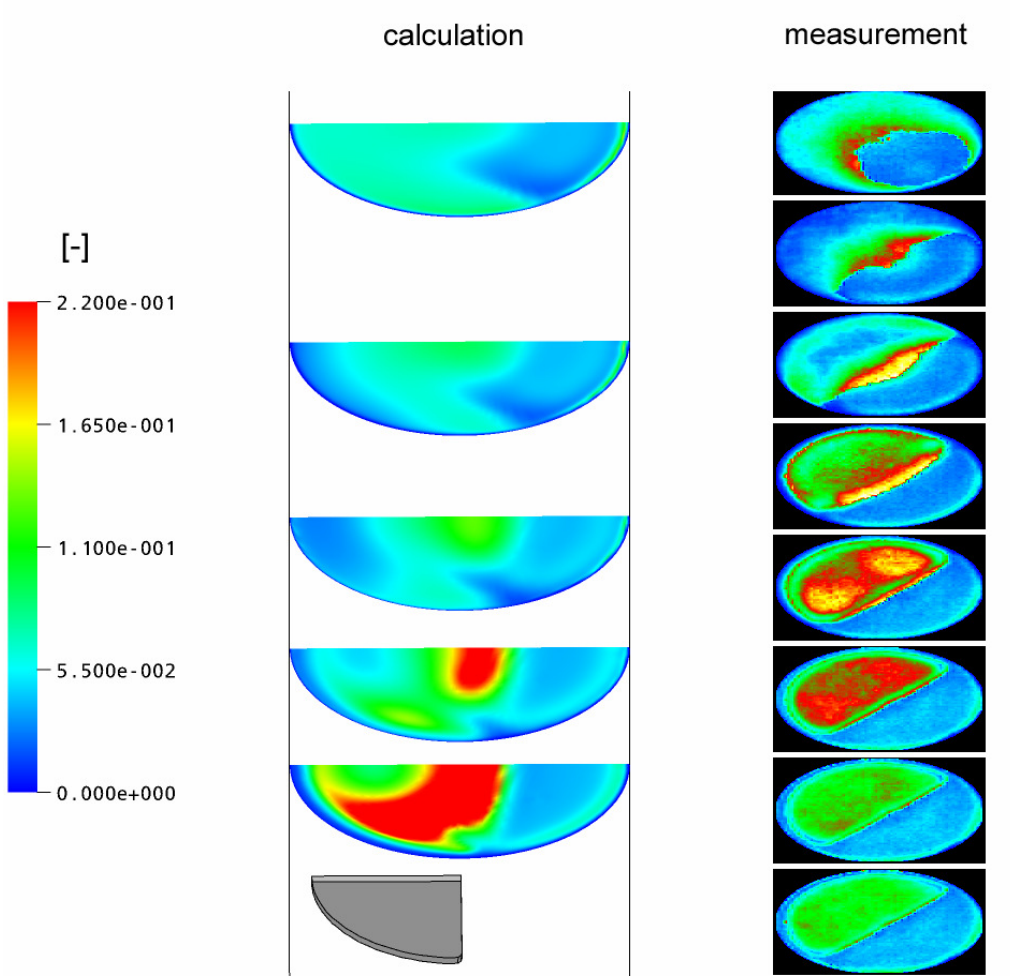

Figure 13: Calculated (left) and measured (right) gas cross fractional distributions downstream the obstacle (run 097: J_L = 1.611 m/s, J_G = 0.0898 m/s);
Calculations (obstacle shown), distances at the axial positions z = 0.08 m, 0.16 m, 0.25 m, 0.37 m and 0.52 m
Measurements (obstacle in the upper left area) distances at z = 0.01 m, 0.015 m, 0.02 m, 0.04 m, 0.08 m, 0.16 m, 0.25 m and 0.52 m

4.3. Phenomena in the jet

In the cross sectional area beside the obstacle a strong jet is established creating strong shear flow. The resulting phenomena are more pronounced with increasing water velocity. Therefore, run 097 is considered, where the liquid velocity was increased to J_L = 1.611 m/s. Fig. 13 presents measured and calculated cross sectional gas fraction distributions for this run. In the most downstream cross section of the measurements an almost gas bubble free region is found. This effect is seen in air/water measurements with J_L >= 1.017 m/s and J_G <= 0.14 m/s but not in the steam/water tests. The streamline representation of the calculations however (Fig. 10 for run 096 which is quite similar to run 097), indicate large bubbles being directed into the jet caused by the lift force.
This discrepancy between experiment and calculation can possibly be explained by the strong water velocity gradient near the jet. This strong shear flow induces bubble fragmentation which is not yet considered in the model of Luo and Svendsen (1996). In the tests, the big bubbles migrate towards the jet, but are fragmented at the relatively sharp boarder of this jet. Only a small fraction of the small bubbles created by this breakup process can enter the jet by action of the turbulent dispersion force.

5. Summary and conclusions

Applying the inhomogeneous MUSIG approach a more deep understanding of the flow structure is possible. For upward two phase flow in vertical pipes the core peak in the cross sectional gas fraction distribution could be reproduced very well. While the closure models on bubble forces, which are responsible for the simulation of bubble migration, are in agreement with the experimental observations, clear deviations occur for bubble coalescence and break-up. The presently applied models describing bubble break-up and coalescence could be proved as weak points in numerous CFD analyses of vertical upward two phase pipe flow. Further work on this topic is under way.

Acknowledgements

The work is carried out as a part of current research projects funded by the German Federal Ministry of Economics and Labour, project numbers 150 1265 and 150 1329. The authors express their gratitude to the technical TOPFLOW team.

References

Bothe, D., M. Schmidtke, H.-J. Warnecke (2006). VOF-Simulation of the Lift Force for Single Bubbles in a Simple Shear Flow. Chem. Eng. Technol. 29, No. 9, 1048–1053.

Burns, A. D., T. Frank, I. Hamill J.-M. Shi (2004). The Favre Averaged Drag Model for Turbulent Dispersion in Eulerian Multi-Phase Flows. 5th International Conference on Multiphase Flow, ICMF'04, Yokohama, Japan, May 30–June 4, 2004, Paper No. 392.

Ervin, E.A., Tryggvason, G. (1997). The rise of bubbles in a vertical shear flow. J.l of Fluids Engineering, vol. 119, pp. 443-449.

Frank, T., Zwart, P.J., Shi, J.-M., Krepper, E., Rohde, U. (2005). Inhomogeneous MUSIG Model – a Population Balance Approach for Polydispersed Bubbly Flows. International Conference "Nuclear Energy for New Europe 2005", Bled, Slovenia, September 5-8, 2005.

Frank, Th., Zwart, P.J., Krepper, E., Prasser, H.-M., Lucas, D., (2006). Validation of CFD models for mono- and polydisperse air-water two-phase flows in pipes. OECD/NEA International Workshop on The Benchmarking of CFD Codes for Application to Nuclear Reactor Safety (CFD4NRS), 05.-09.09.2006, Garching, Deutschland, OECD/NEA, 05.-09.09.2006, Garching, Germany.

Frank, Th., Prasser, H.-M., Beyer, M., Al Issa, S., (2007). Gas-liquid flow around an obstacle in a vertical pipe – CFD simulation & comparison to experimental data. 6th Int. Conf. on Multiphase Flow Leipzig 2007, paper 135.

Krepper, E.; Lucas, D.; Prasser, H.-M., (2005). On the modelling of bubbly flow in vertical pipes. Nuclear Engineering and Design 235 (2005) 597-611.

Krepper, E., Frank, Th., Lucas, D. Prasser, H.-M., Zwart, Ph. J., (2007). Inhomogeneous MUSIG Model – a Population Balance Approach for Polydispersed Bubbly Flows. 6th Int. Conf. on Multiphase Flow Leipzig 2007, paper 375.

Lo S., (1996). Application of the MUSIG model to bubbly flows. AEAT-1096, AEA Technology, June 1996.

Luo, H. and Svendsen, H.F., (1996). Theoretical model for drop and bubble break-up in turbulent flows. AIChEJ, 42, 5, pp. 1225-1233.

Prasser, H.-M., Krepper, E., Lucas, D., (2002). Evolution of the two-phase flow in a vertical tube - decomposition of gas fraction profiles according to bubble size classes using wire-mesh sensors. International Journal of Thermal Sciences, 41 (2002) 17-28.

Prasser, H.-M.; Beyer, M.; Carl, H.; Gregor, S.; Lucas, D.; Pietruske, H.; Schütz, P.; Weiss, F.-P., (2007). Evolution of the structure of a gas-liquid two-phase flow in a large vertical pipe. Nuclear Engineering and Design (accepted for publication).

Prince, M.J. and Blanch, H.W., (1990). Bubble coalescence and break-up in air-sparged bubble columns. AIChEJ, 36, No 10, pp. 1485-1499.

Shi, J.-M., Zwart, P.-J., Frank, T., Rohde U. and Prasser, H.-M., (2004). Development of a multiple velocity multiple size group model for poly-dispersed multiphase flows. In Annual Report of Institute of Safety Research. Forschungszentrum Rossendorf, Germany, 2004.

Tomiyama, A., Sou, I., Zun, I., Kanami, N., Sakaguchi, T., (1995). Effects of Eötvös number and dimensionless liquid volumetric flux on lateral motion of a bubble in a laminar duct flow. Advances in Multiphase Flow, pp. 3-15.

Tomiyama A., (1989). Struggle with computational bubble dynamics. ICMF'98, 3rd Int. Conf. Multiphase Flow, Lyon, France, pp. 1-18, June 8.-12. 1998.

Wellek, R.M., Agrawal, A.K., Skelland, A.H.P., (1966). Shapes of liquid drops moving in liquid media. AIChE Journal, vol. 12, pp. 854-860.

Zwart, P., A. Burns, A. and Montavon C.. (2003). Multiple size group models. Technical report, AEA Technology plc, Novermber, 2003. CFX-5.7.